MOLECULAR AND CELLULAR BIOLOGY, Sept. 2002, p. 6487–6497 Vol. 22, No. 18
0270-7306/02/$04.00+0 DOI: 10.1128/MCB.22.18.6487–6497.2002

Rab3D Is Not Required for Exocrine Exocytosis but for Maintenance of Normally Sized Secretory Granules

Dietmar Riedel,[1] Wolfram Antonin,[1] Rafael Fernandez-Chacon,[2] Guillermo Alvarez de Toledo,[2] Tobias Jo,[1] Martin Geppert,[3]† Jack A. Valentijn,[4] Karin Valentijn,[5] James D. Jamieson,[5] Thomas C. Südhof,[6] and Reinhard Jahn[1]*

Department of Neurobiology, Max Planck Institute for Biophysical Chemistry, 37077 Göttingen,[1] and Department of Molecular Neurobiology, Max Planck Institute for Experimental Medicine, 37073 Göttingen,[3] Germany; Department of Medical Physiology and Biophysics, School of Medicine, University of Seville, 41009 Seville, Spain[2]; Department of Cell Biology, Yale University School of Medicine, New Haven, Connecticut 06510[5]; Department of Biochemistry, Cell Biology and Histology, Faculty of Veterinary Medicine, University of Utrecht, 3584 CL Utrecht, The Netherlands[4]; and Center for Basic Neuroscience, Department of Molecular Genetics, and Howard Hughes Medical Institute, Southwestern Medical Center, University of Texas, Dallas, Texas 75390[6]

Received 19 February 2002/Returned for modification 24 April 2002/Accepted 12 June 2002

Rab3D, a member of the Rab3 subfamily of the Rab/ypt GTPases, is expressed on zymogen granules in the pancreas as well as on secretory vesicles in mast cells and in the parotid gland. To shed light on the function of Rab3D, we have generated Rab3D-deficient mice. These mice are viable and have no obvious phenotypic changes. Secretion of mast cells is normal as revealed by capacitance patch clamping. Furthermore, enzyme content and overall morphology are unchanged in pancreatic and parotid acinar cells of knockout mice. Both the exocrine pancreas and the parotid gland show normal release kinetics in response to secretagogue stimulation, suggesting that Rab3D is not involved in exocytosis. However, the size of secretory granules in both the exocrine pancreas and the parotid gland is significantly increased, with the volume being doubled. We conclude that Rab3D exerts its function during granule maturation, possibly by preventing homotypic fusion of secretory granules.

Rab proteins are small GTPases that belong to the Ras protein superfamily and that function in membrane traffic. In *Saccharomyces cerevisiae*, 11 members of the Rab family (also referred to as ypt/sec4 proteins) are known that operate in distinct intracellular trafficking steps (40). In the human genome, 60 genes coding for Rab proteins have been identified (12).

In recent years, major progress has been made in unraveling the GTP-GDP cycle of Rab proteins. Like Ras, Rab proteins contain an effector domain that undergoes major conformational changes during GTP hydrolysis (44, 53). Cycling between the GTP and GDP form requires additional proteins including GTPase-activating proteins and guanine nucleotide exchange factors (for recent reviews see references 46, 52, and 57). Furthermore, the GTP-GDP cycle is linked to membrane association and dissociation, which involve proteins such as GDP dissociation inhibitor (GDI) and membrane receptors such as Yip proteins. Generally, the GTP form of Rab proteins is considered to be the active form that specifically interacts with effector proteins. For several Rabs such effector proteins have been identified, but in many cases their function is not understood. An increasing body of evidence suggests that individual Rab proteins may interact with multiple effectors that are structurally diverse and that may control different reactions in membrane traffic.

The first clues to the function of Rabs were obtained from yeast mutants with defects in various Rab/ypt proteins. Such defects generally resulted in the accumulation of vesicles at different stages in membrane traffic, suggesting that they are required for membrane fusion. Subsequent studies revealed that Rabs most probably are involved in the initial binding of membranes destined to fuse, a process generally referred to as tethering. According to this view, Rab proteins exert their function before the actual fusion reaction.

Rab3A is one of the best-characterized Rab proteins. In mammals, three additional isoforms are expressed which are referred to as Rab3B, Rab3C, and Rab3D. Rab3A, Rab3B, and Rab3C are predominantly expressed in the nervous system (21, 33), where they are localized to synaptic vesicles. Surprisingly, Rab3A is not essential, since its deletion in mice resulted in a relatively mild phenotype (22). It is unlikely that this is due to isoform redundancy since, in *Caenorhabditis elegans*, which contains only one Rab3 isoform, Rab3 is also not essential, although more pronounced effects on synaptic function and synaptic morphology were observed (39). Electrophysiological analysis of synaptic transmission in neurons of Rab3A-deficient mice revealed that neither the size nor the refilling rate of the readily releasable pool was changed. In contrast, more exocytotic events were observed in response to stimulation, which resulted in an enhanced rundown of synaptic transmission (23). These findings are difficult to reconcile with a func-

* Corresponding author. Mailing address: Department of Neurobiology, Max Planck Institute for Biophysical Chemistry, Am Fassberg 11, 37077 Göttingen, Germany. Phone: 49-551 201 1634. Fax: 49-551 201 1639. E-mail: rjahn@gwdg.de.
† Present address: Pharmacia Corporation, Kalamazoo, MI 49007.

tion of Rab3 in vesicle tethering at the synapse but suggest rather a function intimately associated with fusion. The readily releasable pool represents vesicles that are attached to the plasma membrane and primed for fusion, a pool that is expected to be reduced when tethering is defective.

Unlike Rab3A, Rab3B, and Rab3C, Rab3D is predominantly expressed outside the nervous system. Originally identified in fat cells (7), Rab3D protein is present in several additional cell types, including secretory cells such as pancreatic (42, 55) and parotid (42) acinar cells, mast cells (41), and peptide-secreting cell lines (9). In secretory cells, Rab3D appears to be predominantly localized to secretory granules, thus mirroring the distribution of Rab3A in neurons and neuroendocrine cells. However, in cell types expressing both Rab3A and Rab3D, such as adipocytes, AtT20 cells, and mast cells (RBL-2H3), the two Rab3 forms appear to be differentially localized (8, 36, 49).

Several approaches were made to address the function of Rab3D. In RBL cells (a mast cell line) (15, 49) and AtT20 cells (9), overexpression of wild-type Rab3D or a variant deficient in guanine nucleotide binding results in a reduction of evoked exocytosis. Furthermore, the number of granules close to the plasma membrane was reduced whereas (at least in PC12 cells) overexpression of wild-type protein had the opposite effect, suggesting that Rab3D may be involved in vesicle-membrane interactions, i.e., well before membrane fusion (35). In another approach a transgenic mouse line was created in which Rab3D was selectively overexpressed in the exocrine pancreas, yielding approximately twofold-increased levels of the protein (43). The initial rate of secretagogue-induced enzyme release was doubled in the overexpressing line but reached normal levels after 30 min of stimulation. Together, these results suggest that Rab3D exerts a stimulatory role on exocytosis in various nonneuronal cells, although it is not clear whether the protein is involved in vesicle fusion, vesicle docking, or vesicle maturation.

To shed light on the role of Rab3D, we have now knocked out the Rab3D gene in mice. Surprisingly, Rab3D-deficient mice were viable and fertile and showed no obvious defects. In particular, both kinetics and dose response of secretagogue-induced enzyme secretion of the pancreas were normal. Furthermore, no difference was observed in mast cell degranulation as monitored by capacitance patch clamping. However, electron microscopy revealed that the size of secretory granules in both the exocrine pancreas and the parotid gland is significantly increased, with the volume being doubled, suggesting that Rab3D functions in granule maturation but not in exocytotic membrane fusion.

MATERIALS AND METHODS

Antibodies. Monoclonal antibodies specific for Rab3A (Cl42.2 [37]), syncollin (Cl87.1 [2]), synaptobrevin 2 (Cl69.1 [16]), GDI (Cl81.1 [14]), and rabphilin (clone Cl76.2 [5]) as well as polyclonal antibodies specific for Rab3B (O. M. Schluetter et al., unpublished data); Rab3C (20); endobrevin (19); and syntaxins 2, 3, 4, 7, and 13 were described previously (4, 5, 25) and are commercially available from Synaptic Systems (Göttingen, Germany). Cellubrevin (3) and syntaxin 8 (4) antisera were described previously.

Antibodies specific for secretory carrier membrane protein (SCAMP) and synaptosome-associated protein 23 (SNAP-23) were obtained from Synaptic Systems. Antibodies specific for β-tubulin and syntaxin 6 were obtained from Sigma, (Deisenhofen, Germany) and from Transduction Laboratories (San Diego, Calif.), respectively.

A rabbit serum specific for Rab3D (no cross-reactivity toward other Rab3 isoforms) was raised against a synthetic C-terminal peptide (C-NGKPALGDT P).

Generation of Rab3D-deficient mice. Rab3D mutant mice were generated by homologous recombination in embryonic E14.1 stem cells derived from the mouse line 129Sv/J as described before (51). In short, three genomic clones containing coding exons of murine Rab3D were isolated from a λFixIISV129 mouse genomic library (Stratagene, La Jolla, Calif.) by standard techniques. The gene-targeting vector based on these clones replaced the first exon of Rab3D (amino acids 1 to 76; see Fig. 1) with a neomycin resistance cassette. A 4.4-kbp *Bam*HI-*Not*I fragment was cloned into the same sites of pTKneo3A. A 4.7-kbp blunt-ended *Cla*I/*Not*I fragment was ligated into the polished *Cla*I site of the vector. Following electroporation and selection, recombinant stem cells were analyzed by Southern blotting. For hybridization, an outside probe localized 3′ of the targeting vector short arm was used. Positive clones were injected into C57BL6/J mouse blastocysts to obtain highly chimeric mice that transmitted the mutation through the germ line. Germ line transmission was confirmed by Southern blotting. Subsequent genotyping was performed by PCR with primer pairs specific for the wild-type allele (5′-GCCATCTCTCCAGCCCTTGTTT GTC and 5′-CTCCAGTTATGTAGGCAAGGCTAGCC) or the mutant allele (5′-CCTGTCCGGTGCCCTGAATGAA and 5′-GCCGATCCCCTCAGAAGA AC), both generating fragments of 550 bp. Mice were backcrossed to C57BL6/J mice, bred, and maintained by standard mouse husbandry procedures.

Electrophysiological analysis of mast cells. Mast cells were obtained essentially as described elsewhere (1, 21) from wild-type and Rab3D-knockout (KO) mice by peritoneal lavage with buffer A (140 mM NaCl, 10 mM HEPES-NaOH, 2 mM $CaCl_2$, 1 mM $MgCl_2$, 6 mM glucose, and 45 mM $NaHCO_3$, pH 7.2). Cells were plated on coverslips and incubated in an atmosphere of 5% CO_2–95% air until use (between 1 and 8 h after culture). All experiments were performed at room temperature in buffer A without $NaHCO_3$; glucose was added to adjust the osmolarity. Patch pipette solutions contained 140 mM potassium glutamate, 10 mM HEPES, 7 mM $MgCl_2$, 3 mM KOH, 0.2 mM Mg-ATP, 2.5 mM K_2-EGTA, and 7.5 mM Ca-EGTA. The final Ca^{2+} concentration was between 500 and 900 nM. We added 5 μM GTPγS to the pipette solution to induce degranulation. Mast cells were identified, and degranulation was visually monitored with an inverted microscope (IM-35; Zeiss) equipped with Nomarski optics. Membrane capacitance was measured by whole-cell recordings (24). The C-slow and G-series potentiometers of an EPC-8 (Heka Electronics) patch clamp amplifier were used to cancel out the incoming membrane current in order to resolve small capacitance changes. Direct readout of these knobs gave us the approximations for the initial and final cell membrane capacitance and series conductance of every cell. We obtained a calibration signal by unbalancing the C-slow potentiometer by 100 fF, corresponding to a change of 10 μm^2 (assuming a specific membrane capacitance of 1 $\mu F/cm^2$ of membrane). The V-command was a 50-mV sine wave (root mean square, 1 kHz). Capacitance and conductance values were estimated from the real and imaginary components of the complex admittance, which was obtained by a Lock-In amplifier (SR-830; Stanford Research) (34). Data acquisition was done using an IDA 15125 board (INDEC Systems) programmed in Visual Basic. One data point was obtained every 2.5 ms. Data analysis was done with IGOR Pro 4.01 (Wavemetrics). Vesicle radii were calculated assuming that a vesicle is spherical and its specific membrane capacitance is 1 $\mu F/cm^2$.

Electron microscopy. To perform morphological studies, 600-nm-thick sections of EMbed 812 (Plano)-embedded tissue, described below, were stained with toluidine blue and visualized in a Zeiss light microscope.

For transmission electron microscopy pieces of pancreas no larger than 2 mm^3 were fixed by immersion with 2% glutaraldehyde in 0.1 M cacodylate buffer at pH 7.4. After postfixation in 1% osmium tetroxide on ice and preembedding staining with 1% tannic acid and 1% uranyl acetate, tissue samples were dehydrated and embedded in EMbed 812. Thin sections were counterstained with lead citrate and examined with a Philips CM 120 BioTwin transmission electron microscope (Philips Inc., Eindhoven, The Netherlands). Images were taken with a 1K slow-scan charge-coupled device camera (GATAN, Inc.).

Purified zymogen granules from a sucrose gradient (see below) were centrifuged for 10 min at 4,000 rpm in a Biofuge (Heraeus). The pellet was diluted with 40 μl of 2% agarose in 0.1 M cacodylate buffer at pH 7.4. Small pieces of the agarose-immobilized granules were cut and used for an EMbed embedding as described above.

Image analysis. The diameters of zymogen granules were measured on digital images taken at the eucentric height at the same magnification and defocus with DigitalMicrograph 3.4 (GATAN, Inc.). Since the shape of the zymogen granules

is elliptical, the short (a) and the long (b) diameters of the granules were measured perpendicular to the membrane. The distribution of the vesicle diameters was done with the mean diameters $c = (a + b)/2$. Only organelles with clearly delineated membranes were measured. The mean diameters of all measured vesicles were corrected by the estimated section thickness of 80 nm by using the theoretical solution given by reference 45. For each calculation sections from two different animals were analyzed.

Subcellular fractionation. Small synaptic vesicles (LP2 fraction) from brain (28) and zymogen granules from pancreas (38) were prepared in the presence of 0.1 mM GTPγS. To enrich for membrane proteins, phase partitioning in Triton X-114 was performed on homogenate fractions (13). For immunoblotting with antibodies specific for syntaxin 2, syntaxin 3, syntaxin 4, syntaxin 7, syntaxin 13, syntaxin 6, syntaxin 8, endobrevin, cellubrevin, SNAP-23, and Rab3D, an aliquot of the detergent phase corresponding to 200 μg of protein of the starting homogenate was loaded per lane, and for SCAMP and synaptobrevin 2, aliquots corresponding to 50 μg of protein of the starting homogenate were loaded per lane. For immunoblotting with antibodies specific for GDI, *N*-ethylmaleimide-sensitive fusion protein (NSF), rabphilin, syncollin, and β-tubulin, 20 μg of homogenate was loaded per lane. Signals were quantified with enhanced chemiluminescence reagent (NEN, Boston, Mass.) and an Image Reader LAS-1000 in combination with AIDA software (Raytest) (see Table 1).

For isopycnic sucrose density gradient centrifugation, zymogen granules were prepared as described previously (38). Zymogen granules derived from one pancreas were resuspended in 300 μl of homogenization buffer (280 mM sucrose, 5 mM morpholineethanesulfonic acid [MES; pH 6.5], 1 mM EDTA, 0.1 mM phenylmethylsulfonyl fluoride [PMSF], 10 μg of soybean trypsin inhibitor/ml, 1 μg of pepstatin/ml, 11 μg of benzamidine/ml, 1 μg of antipain/ml, 1 μg of leupeptin/ml), loaded on top of a continuous sucrose gradient (10 ml of 35 to 60% [wt/vol] sucrose in 5 mM MES [pH 6.5]–1 mM EDTA–0.1 mM PMSF–1 μg of soybean trypsin inhibitor/ml–0.1 μg of pepstatin/ml–1.1 μg of benzamidine/ml–0.1 μg of antipain/ml–0.1 μg of leupeptin/ml), and centrifuged for 19 h at 40,000 rpm in a Beckman (Fullerton, Calif.) SW41 rotor. After centrifugation fractions of 300 μl were collected. All samples were analyzed for amylase (by enzyme assay; see below) (Fig. 1B), for SCAMP and synaptobrevin 2 (by immunoblotting), and for size distribution (by electron microscopy; see above) (see Fig. 5 and 6). The sucrose concentration of each fraction was determined by refractometry.

Secretion of amylase. Secretion was monitored by measuring the release of amylase from pancreatic and parotid lobules (prepared according to the method of reference 50) in response to carbamylcholine and isoproterenol, respectively. For each incubation 20 to 30 lobules were suspended in oxygen-saturated incubation buffer consisting of 20 mM HEPES (pH 7.4), 120 mM NaCl, 5 mM KCl, 1.2 mM $MgCl_2$, 2 mM $CaCl_2$, 14 mM glucose, Eagle's minimal essential medium amino acid supplement, and 2 mM L-glutamine. Amylase discharge into the incubation medium was expressed as percentage of total amylase content in the lobules at the beginning of the incubation.

Protein synthesis and transport. To measure discharge of radioactively labeled proteins, lobules were incubated for 10 min in Dulbecco modified Eagle medium supplemented with amino acids and 500 μCi of ^{3}H-labeled amino acids (TRK440; Amersham)/ml, washed, and transferred into unlabeled medium. Where indicated, the medium contained 0.5 μM carbachol. At the indicated time points, aliquots of medium and lobules were removed, and the lobules were homogenized in lysis buffer (20 mM Tris-HCl [pH 9.0], 0.01% Triton X-100, 0.1 mM PMSF, 1 μg of soybean trypsin inhibitor/ml, 0.1 μg of pepstatin/ml, 1.1 μg of benzamidine/ml, 0.1 μg of antipain/ml, 0.1 μg of leupeptin/ml). Protein synthesis was measured by determination of trichloroacetic acid-insoluble radioactivity of the homogenate samples normalized to the DNA content. Discharge of labeled protein was measured by quantifying the trichloroacetic acid-insoluble radioactivity of the medium. In all cases, radioactivity was determined by liquid scintillation counting. In all experiments, lactate dehydrogenase released into the medium remained constant during the incubation time, showing that protein release is not caused by nonspecific tissue damage.

Other methods. Trypsin was measured after activation by enterokinase (50) according to the method in reference 27 using *N*-benzoyl arginine ethyl ester as substrate. Chymotrypsin was assayed after activation by trypsin with benzoyl tyrosine ethyl ester as substrate (27). Amylase was measured according to the method in reference 11, and lactate dehydrogenase was measured according to the method in reference 10. Protein was determined by the bicinchoninic acid method (Pierce) according to the instructions of the manufacturer. All enzyme activities were normalized to the DNA content (determined according to the method in reference 48) of the homogenate.

RESULTS

A murine genomic library was screened with mouse Rab3D cDNA as a probe to isolate genomic clones of the murine Rab3D locus. Three independent clones were isolated which contained the first coding exon of mouse Rab3D.

The targeting vector for homologous recombination replaced exon 1 (coding for residues 1 to 76 of Rab3D) with a neomycin resistance cassette (Fig. 1A). Electroporation of the targeting vector into E14.1 mouse embryonic stem cells (26) resulted in clones in which homologous recombination of the Rab3D gene had occurred. Chimeric mice were generated by blastocyst injection with one of the stem cell clones. These mice were used for breeding to generate heterozygous mutant mice. Interbreeding of the heterozygous mice resulted in offspring that showed the predicted Mendelian frequencies of wild-type, heterozygous, and homozygous genotypes.

Mice lacking the Rab3D gene were viable and fertile and exhibited no obvious phenotypic changes. Mutant mice were capable of reproducing and of caring for their offspring. Their body weights and their life spans were comparable to those of their wild-type and heterozygous littermates. To confirm that no Rab3D protein was expressed, we performed an immunoblot analysis of pancreatic zymogen granules, isolated from adult mice, which are known to be enriched in Rab3D protein (Fig. 1B). Rab3D was not detectable in homozygous mutants, whereas the levels of synaptobrevin and SCAMP, two integral membrane proteins of zymogen granules, were normal. Furthermore, Rab3A, Rab3B, and Rab3C were not detectable in wild-type or Rab3D-deficient mice, whereas a synaptic vesicle preparation from mouse brain showed strong signals for these three Rab3 isoforms.

As outlined in the introduction, both the localization of Rab3D to secretory organelles and previous functional studies strongly suggest that the protein plays an important role in regulated exocytosis. We have therefore concentrated our analysis on secretory cells, focusing on mast cells and exocrine glands in which such a role was inferred from previous studies. Peritoneal mast cells were isolated from mutant and wild-type mice. When analyzed by light microscopy, the two cell populations were similar and exhibited no obvious morphological alterations (data not shown). To investigate whether exocytosis was affected, we performed whole-cell capacitance patch clamping experiments. This procedure not only allows for high kinetic resolution of release but also permits an accurate determination of the vesicle size. Degranulation was induced by GTPγS, which was included in the pipette solution (see Materials and Methods). As shown in Fig. 2A and B, no difference in the kinetics of exocytosis was observed between mast cells derived from Rab3D-deficient mice and littermate controls. Furthermore, Rab3D-deficient mast cells appeared to possess a normal inventory of granules, since the relative capacitance increase (which is a measure of the total surface area of all exocytosed granules with respect to the cell size) was not changed. We also compared the size distribution of individual capacitance step increases (Fig. 2C and D), which are a direct measure of vesicle size (Fig. 2E and F). Again, no significant differences were observed between Rab3D-deficient and control cells. We conclude that, in contrast to previous assump-

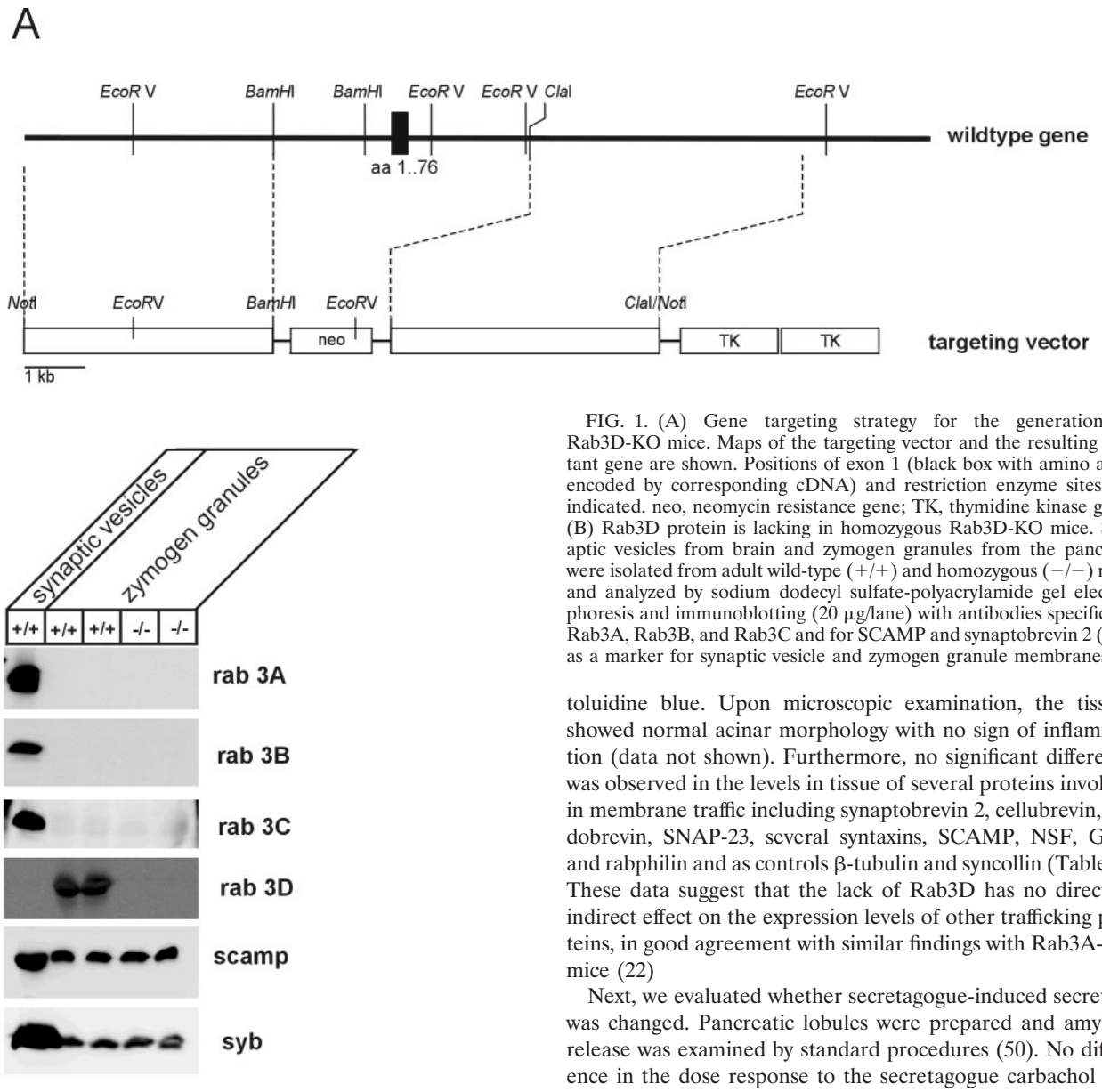

FIG. 1. (A) Gene targeting strategy for the generation of Rab3D-KO mice. Maps of the targeting vector and the resulting mutant gene are shown. Positions of exon 1 (black box with amino acids encoded by corresponding cDNA) and restriction enzyme sites are indicated. neo, neomycin resistance gene; TK, thymidine kinase gene. (B) Rab3D protein is lacking in homozygous Rab3D-KO mice. Synaptic vesicles from brain and zymogen granules from the pancreas were isolated from adult wild-type (+/+) and homozygous (−/−) mice and analyzed by sodium dodecyl sulfate-polyacrylamide gel electrophoresis and immunoblotting (20 μg/lane) with antibodies specific for Rab3A, Rab3B, and Rab3C and for SCAMP and synaptobrevin 2 (syb) as a marker for synaptic vesicle and zymogen granule membranes.

tions, Rab3D is not involved in mast cell degranulation or in the establishment of secretion-competent vesicle pools.

We next investigated whether the function of exocrine glands is affected in Rab3D-deficient mice, with the main emphasis being on the exocrine pancreas. In pancreatic acinar cells, Rab3D is localized on the membrane of zymogen granules (42, 55). Upon stimulation, the protein has previously been shown to undergo major redistribution to recycling membranes but appears to be absent from the apical plasma membrane (32). These data suggested that membrane dissociation, and thus perhaps also GTP hydrolysis, is associated with exocytosis and thus may be involved in its regulation.

No obvious gross morphological changes were observable in the pancreata of Rab3D-deficient mice. From both the pancreas and the parotid glands of 90-day-old homozygous mutant mice semithin sections were prepared that were stained with toluidine blue. Upon microscopic examination, the tissues showed normal acinar morphology with no sign of inflammation (data not shown). Furthermore, no significant difference was observed in the levels in tissue of several proteins involved in membrane traffic including synaptobrevin 2, cellubrevin, endobrevin, SNAP-23, several syntaxins, SCAMP, NSF, GDI, and rabphilin and as controls β-tubulin and syncollin (Table 1). These data suggest that the lack of Rab3D has no direct or indirect effect on the expression levels of other trafficking proteins, in good agreement with similar findings with Rab3A-KO mice (22)

Next, we evaluated whether secretagogue-induced secretion was changed. Pancreatic lobules were prepared and amylase release was examined by standard procedures (50). No difference in the dose response to the secretagogue carbachol was observed between Rab3D-deficient mice and littermate controls showing a maximum at a carbachol concentration of 0.5 μM (Fig. 3A). To exclude differences in the release kinetics, the time dependence of amylase release was monitored. As shown in Fig. 3B, no differences in basal and evoked secretion were found regardless of whether lobules were stimulated by submaximal (0.1 μM) or maximal (0.5 μM) carbachol concentrations. We also tested whether Rab3D is involved in the control of amylase release in the parotid gland as suggested by several previous publications (42, 47). However, again no differences in the extent of evoked amylase release were observed between Rab3D-deficient mice and littermate controls when secretion was stimulated for 60 min with an 0.3 μM concentration of the β-adrenergic agonist isoproterenol: 81.9% of total amylase was released in wild-type mice versus 80.1% in Rab3D-deficient mice ($n = 4$ for each genotype with a range of 78.2 to 84.2% for wild-type mice and 76.6 to 83.3% for KO mice). Similarly, basal secretion over a period of 60 min was

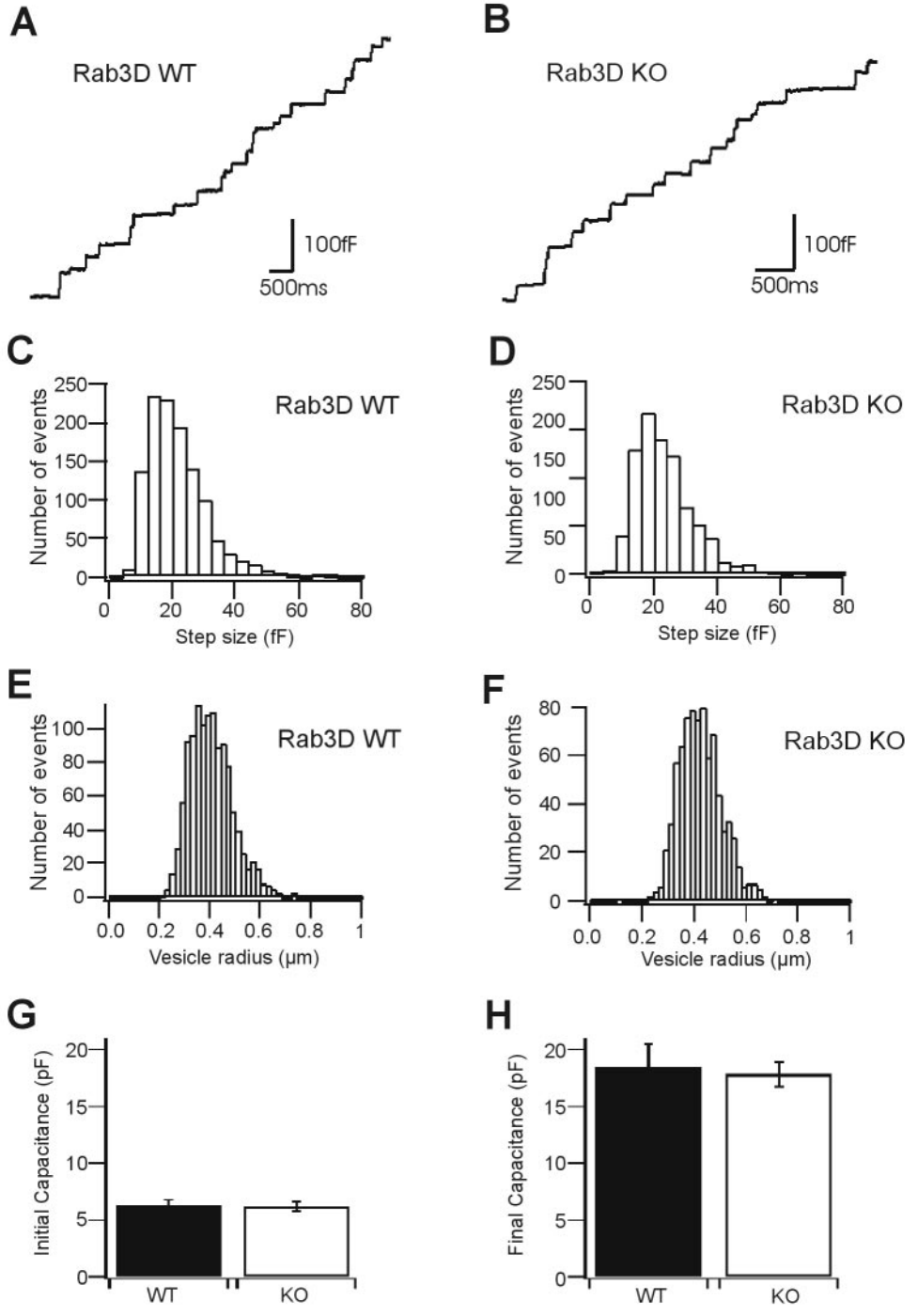

FIG. 2. Exocytosis and granule size of mast cell granules, measured as step increase of membrane capacitance, are unchanged in Rab3D-deficient mice. (A and B) Representative traces of vesicle fusion in mast cells isolated from wild-type and Rab3D-deficient mice, respectively. Stepwise increases of membrane capacitance typically identify exocytotic events of single vesicles. (C to F) Size distributions of secretory vesicles. Panels C and D show step size histograms of discrete and irreversible increases of membrane capacitance (wild-type [WT] cells [C], 21.3 ± 0.27 fF [mean ± standard error of the mean], n = 1,186; mutant cells [D], 23.15 ± 0.32 fF, n = 799). Panels E and F show the distribution of vesicle radii (wild-type cells [E], 0.40 ± 0.002 μm, n = 1,186; mutant cells [F], 0.42 ± 0.003 μm, n = 799). Data were obtained from seven cells derived from two wild-type mice and six cells from two mutant mice. (G) Initial plasma membrane capacitance in mast cells measured immediately before intracellular stimulation of exocytosis with GTPγS (wild-type cells, 6.22 ± 0.55 pF [mean ± standard error of the mean], from 14 cells derived from two mice; mutant cells, 6.17 ± 0.42 pF, from 17 cells derived from three mice). (H) Final cell membrane capacitance after stimulation of exocytosis with GTPγS (wild-type cells, 18.46 ± 2.04 pF, from 13 cells derived from two mice; mutant cells, 17.80 ± 1.12 pF, from 17 cells derived from three mice).

TABLE 1. Levels in pancreatic tissue of Rab3D and proteins involved in membrane traffic[a]

Protein	% (Range) of protein in mouse type:	
	+/+	−/−
Synaptobrevin 2	100 (96.3–103.4)	97.9 (92.9–105.2)
SNAP-23	100 (95.9–105.4)	120.1 (117.8–124.1)
Cellubrevin	100 (92.4–111.6)	92.2 (82.1–103.6)
Endobrevin	100 (94.1–104.4)	97.9 (95.4–99.5)
Syntaxin 7	100 (91.6–111.1)	102.2 (78.8–117.4)
Syntaxin 13	100 (90.1–117.2)	102.4 (90.1–112.7)
Syntaxin 8	100 (91.8–110.9)	106.8 (98.2–112.3)
Syntaxin 6	100 (85.3–109.6)	91.6 (81.5–98.2)
Syntaxin 2	100 (93.2–105.3)	99.3 (94.5–105.6)
Syntaxin 3	100 (98.3–102.9)	97.3 (90.9–102.9)
Syntaxin 4	100 (92.7–104.1)	94.1 (89.4–100.9)
SCAMP	100 (93.4–105.8)	102.3 (98.4–105.9)
Syncollin	100 (93.3–103.4)	98.5 (90.7–109.5)
NSF	100 (94.6–105.5)	95.5 (89.0–100.0)
GDI	100 (95.7–107.6)	97.9 (95.6–102.1)
β-Tubulin	100 (94.4–106.8)	98.5 (87.8–106.7)
Rabphilin	100 (94.2–107.2)	97.6 (89.6–105.1)
Rab3D	100 (95.5–105.8)	3.9 (1.4–7.9)

[a] Pancreatic proteins derived from wild-type (+/+) and KO (−/−) mice (three mice per group) were analyzed by sodium dodecyl sulfate-polyacrylamide gel electrophoresis and quantitative immunoblotting. Signals were normalized to the signal average of wild-type mice and are given as percentages.

low in unstimulated wild-type and Rab3D-deficient mice (both 14.9%; $n = 4$ for each genotype with a range of 12.6 to 16.1% for wild-type and 13.7 to 17.2% for KO mice).

While these results exclude a direct involvement of Rab3D in exocytosis, it is conceivable that Rab3D is involved at an earlier step in granule biogenesis, which under our experimental conditions was not rate limiting and thus would not become apparent in the release assays. We therefore used established protocols to determine the intracellular transport rate of newly synthesized zymogens. Pancreatic lobules were pulse-labeled for 5 min with radioactive amino acids, washed, and transferred to unlabeled medium, followed by incubation in either the presence or the absence of the secretagogue carbachol. At different time points, the amount of labeled protein was determined in the medium and in the tissue.

Basal discharge of radiolabeled protein was low in unstimulated controls of both wild-type and KO mice (Fig. 4A). Furthermore, no difference in the secretion of labeled protein was observed in the presence of 0.5 μM carbachol. In both wild-type and Rab3A-deficient mouse lobules, discharge of labeled protein commenced 30 min after the beginning of incubation. As expected, the levels in tissue of radiolabeled proteins showed an inverse relationship. After reaching a plateau, the levels in tissue remained unchanged over the entire incubation period in unstimulated control incubations. In the carbachol-containing incubation mixtures, levels in tissue started to decrease after 30 min in lobules prepared from wild-type and Rab3D-deficient mice (Fig. 4B). Together these data show that the intracellular transit time of secretory proteins is unchanged in Rab3D-deficient mice.

We also checked whether the polarity of exocytosis is affected. Acinar cells exhibit a high polarity, and zymogen granules fuse only with the apical plasma membrane. When polarity is disturbed such as in pancreatitis, zymogen granules also fuse

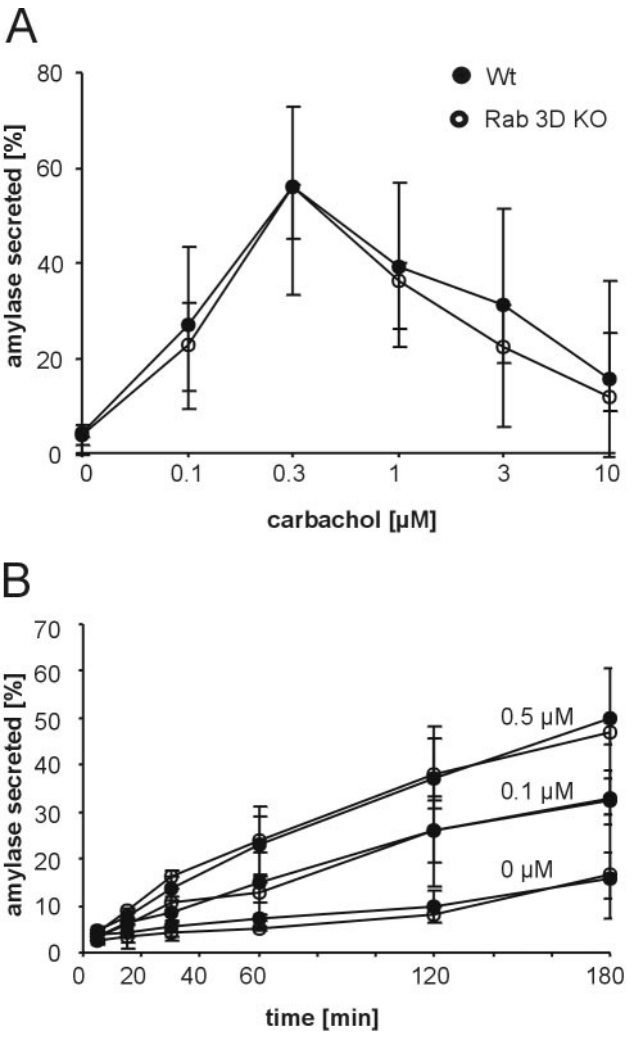

FIG. 3. Amylase release is unchanged in the pancreas of Rab3D-deficient mice. Amylase release was measured with isolated pancreatic lobules prepared from wild-type and KO mice. Secretion is expressed as a percentage of amylase activity released into the medium with respect to total amylase content (sum of amylase discharged in the medium and amylase retained in the tissue). Each value represents the mean of four independent experiments; bars indicate the range. (A) Dose dependence of carbachol-induced amylase release. (B) Discharge kinetics of amylase unstimulated and in response to 0.1 μM and 0.5 μM carbachol.

with the basolateral membrane, resulting in a measurable increase in serum amylase concentration. However, we did not detect any difference in the serum amylase levels between wild-type (100% [72 to 123.3%]) and Rab3D-deficient (94.2% [87.5 to 136.8%]) mice (also Fig. 5C and D).

The experiments described so far revealed no difference in the functional parameters of the secretory pathway between Rab3D-deficient and wild-type control mice. We therefore examined whether the structure of the organelles involved in the secretory pathway was altered, with a special emphasis on secretory granules where Rab3D is normally localized. Small tissue pieces were prepared from randomly selected areas of both the pancreas and the parotid gland. They were fixed by immersion and then processed for transmission electron mi-

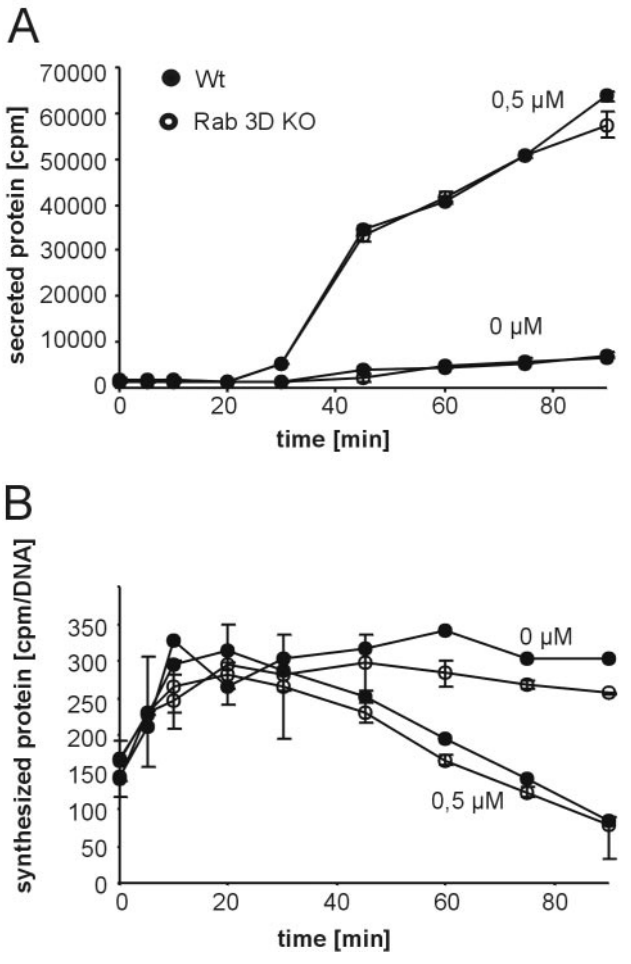

FIG. 4. Intracellular transport of proteins is not affected in the pancreas of Rab3D-deficient mice. Pancreatic lobules derived from wild-type and KO mice were incubated for 5 min in medium containing ^{3}H-labeled amino acids. After chase to cold medium containing either no stimulants (0 μM) or 0.5 μM carbachol, aliquots of the medium (A) and the lobules (B) were removed as indicated, and trichloroacetic acid-precipitable radioactivity was determined. The values were normalized to the DNA content of the homogenates. Values are means of two different animals; bars indicate the range.

croscopy. As already inferred from light microscopic examination of tissue sections, the acini were normally organized and displayed normal polarity. However, the secretory granules in both the exocrine pancreas (Fig. 5C and D) and the parotid gland (Fig. 5A and B) appeared to be larger in Rab3D-deficient mice than in wild-type littermate controls. For quantitation, a large number of granules, approximately 1,000 granules each, were randomly selected from independent sections and measured. As shown in the histograms of Fig. 6, the size distribution of the granules from pancreatic as well as parotid acini was shifted to larger radii in Rab3D-deficient mice (Fig. 5B and D), with an average increase from 431 to 526 nm in the pancreas and from 370 to 453 nm in the parotid gland. When converted into volume, these increases amount to an average doubling of the volume of the secretory granules in both exocrine glands.

According to the classical pathway worked out by Palade and colleagues (44a), secretory granules in exocrine glands are derived from the trans-Golgi network as large, irregularly shaped vacuolar structures. These condensing vacuoles then undergo further maturation involving an increase in intravesicular protein concentration that is associated with a reduction in size. Size reduction involves the removal of membrane, which is probably achieved by budding of small and empty vesicles. The larger size of the secretory granules in Rab3D-deficient mice may thus be due to a defect in granule maturation. To test for this possibility, we performed isopycnic sucrose density gradient centrifugation on preenriched zymogen granule fractions of the pancreas. The density of mature zymogen granules is largely determined by the intracellular protein concentration. If the doubling of the volume is due to a maturation defect, the protein concentration within zymogen granules of Rab3D-deficient mice would be expected to be only half of that of normal mice, which should result in a measurable reduction of their buoyant density.

As shown in Fig. 7, no change in the buoyant density was observed in zymogen granules obtained from Rab3D-deficient mice. To exclude the possibility that the high osmolarity of the sucrose gradient solution influences the shrinkage of zymogen granules derived from KO mice, the zymogen granule fractions were collected from the gradient, pooled, and immediately processed for electron microscopy. When the granule size distribution was determined, the same shift in the size distribution was observed as in the pancreatic tissue (Fig. 6C). We conclude that despite their larger size the density of zymogen granules is not changed in Rab3D-deficient mice, suggesting that the intragranular protein concentration corresponds to that of mature wild-type granules. To exclude the possibility that the overall concentration of zymogen is increased, we determined the pancreatic zymogen levels in Rab3D-deficient mice and littermate controls. No significant differences were observed. The levels of trypsin were unchanged and the levels of chymotrypsin, amylase, and total protein (all calibrated on the DNA content) were slightly reduced in Rab3D-deficient mice (Table 2).

DISCUSSION

In the present study we have addressed the role of Rab3D by generating Rab3D-KO mice. Our data document that the protein is not essential for survival or for basic performance of the major organs. In contrast to previous assumptions, basal and evoked secretion is normal in both mast cells and exocrine glands, suggesting that the protein is obviously not involved in a step crucial for the secretory pathway. Intriguingly, however, we found that in Rab3D-deficient mice the size of enzyme-containing secretory granules in both the pancreas and the parotid gland is drastically increased, suggesting that the protein plays a role in granule maturation.

Due to its high homology to Rab3A, Rab3B, and Rab3C, Rab3D (75.6% identity with Rab3A in mice) was considered to be an isoform, particularly since all Rab3 proteins are localized to secretory organelles involved in regulated exocytosis. Rab3A, which is much better characterized than Rab3D, was therefore assumed to be paradigmatic for all Rab3 isoforms. Despite major efforts, the precise molecular step controlled by Rab3A is still far from clear. The analysis of Rab3A-deficient

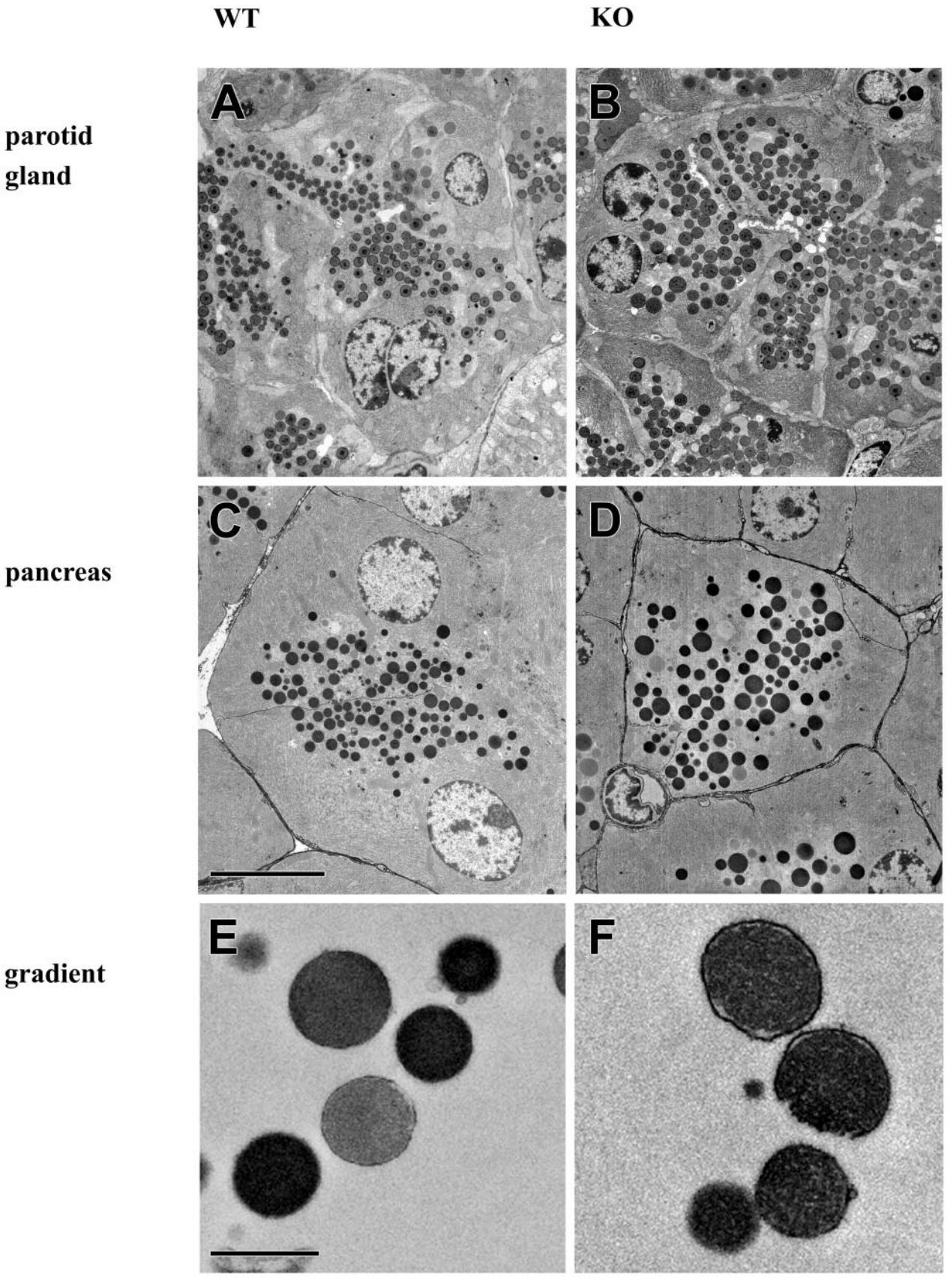

FIG. 5. Electron micrographs obtained from ultrathin sections of parotid gland (A and B) or pancreas (C and D) derived from wild-type (A and C) and Rab3D-deficient (B and D) mice. Also shown are purified zymogen granules derived from a sucrose gradient from wild-type (E) and Rab3D-deficient (F) mice. Bars, 7 (A to D) and 1 (E and F) μm.

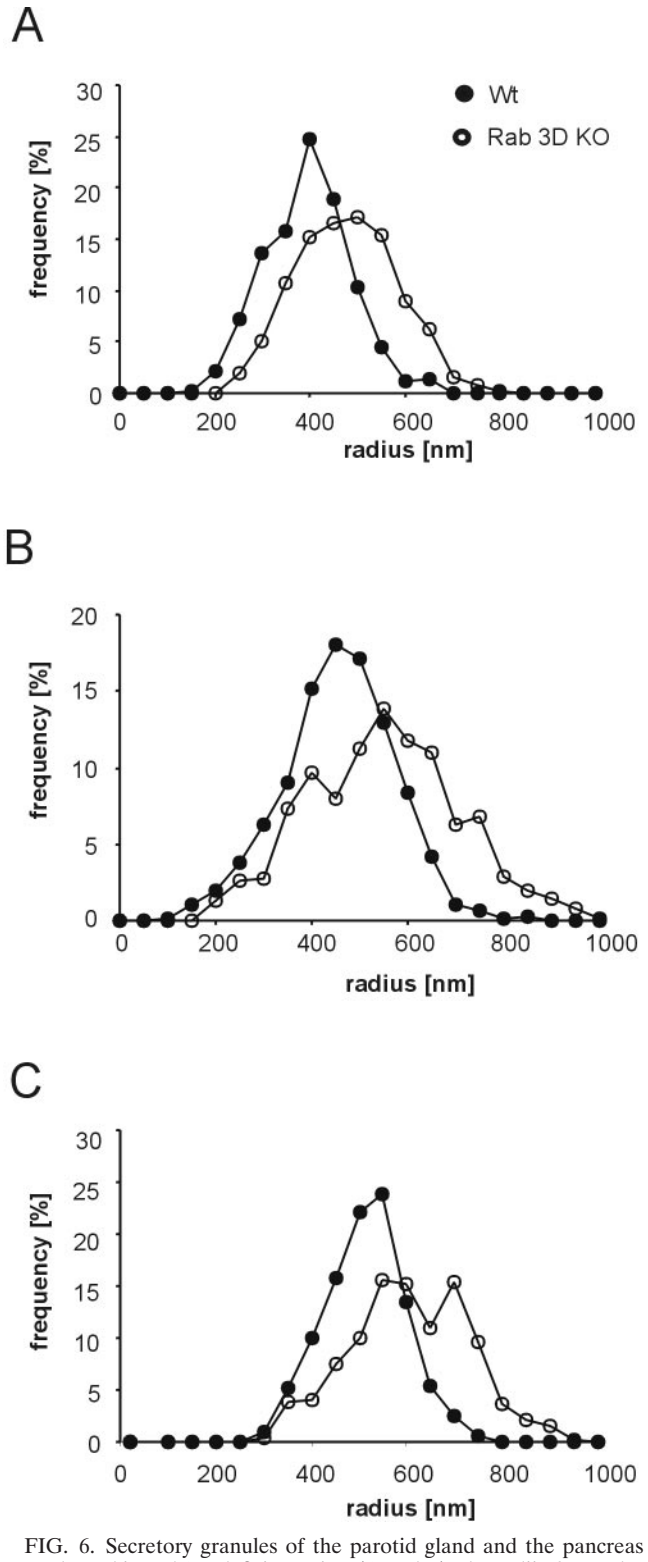

FIG. 6. Secretory granules of the parotid gland and the pancreas are enlarged in Rab3D-deficient mice. (A and B) The radii of granules were measured in ultrathin sections from the parotid gland (A) and the pancreas (B) by using images obtained with a slow-scan charge-coupled device camera. Each data set represents a combination of values obtained from two mice. The values were normalized to the total number of granules. (C) Zymogen granules of Rab3D-deficient mice, purified by sucrose gradient centrifugation, retain the increase in the vesicle diameter after granule isolation.

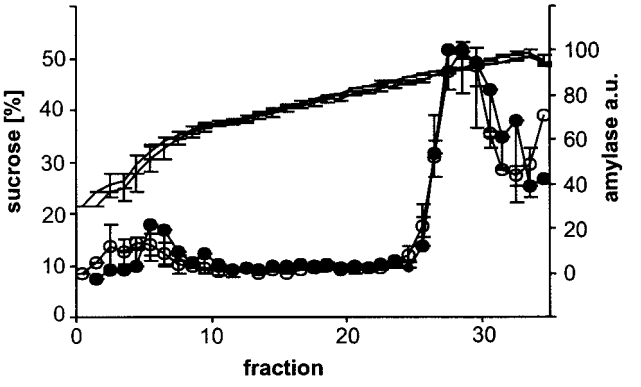

FIG. 7. The buoyant density of zymogen granules is unchanged in Rab3D-deficient mice. Fractions enriched in zymogen granules were subjected to isopycnic sucrose density gradient centrifugation (closed circles, wild-type mice; open circles, Rab3D-deficient mice). The gradient was fractionated in 300-μl aliquots, and the distribution of zymogen granules was measured by determining the amylase content of each fraction. Lines without circles indicate the sucrose concentration of each fraction, determined by refractometry. The values are means of two different experiments; the bars represent the range of the data points. Filled circles, Rab3D-deficient mice; open circles, wild-type controls.

mice suggests that the protein functions close to exocytosis without influencing vesicle recruitment (23). While the presence of additional synaptic Rab3 isoforms in mice may influence the phenotype of Rab3A-deficient mice, only one Rab3 isoform has been identified in the nematode *C. elegans* (12). Therefore, the KO phenotype should be free of problems caused by isoform redundancy. Nematodes lacking functional Rab3 are viable but are characterized by depressed neurotransmitter release (39). Furthermore, unlike in Rab3A-deficient mice the number of synaptic vesicles in nerve terminals is significantly reduced. Based on these findings, it was suggested that Rab3 may regulate vesicle recruitment, but a function in the fusion step cannot be excluded. Similar effects were also observed for aex-3 (the Rab3 GDP-GTP exchange protein) mutants in whom Rab3 is mislocalized (30), although Rab3-independent function of aex-3 cannot be ruled out (31). It should be noted that the function of Rab3 proteins has also been investigated in secretory cell lines by using overexpression of wild-type or mutant proteins deficient either in GTP hydrolysis or in guanine nucleotide binding (9, 29, 35, 49). A variety of effects have been reported, including both inhibition and

TABLE 2. Protein and enzyme levels in the pancreata of wild-type and Rab3D-deficient mice[a]

Protein or enzyme	% (Range) in mouse type:	
	+/+	−/−
Protein	100 (76–130)	87 (75–94)
Chymotrypsin	100 (89–119)	67 (57–76)
Trypsin	100 (66–131)	96 (74–122)
Amylase	100 (70–123)	76 (64–85)

[a] +/+, wild type; −/−, Rab3D deficient. Protein levels and enzyme activities were normalized to DNA content. Four mice of each genotype were analyzed. The means of wild-type values were set to 100%.

stimulation of exocytosis, but no coherent picture has emerged from these studies.

In contrast to Rab3A, Rab3B, and Rab3C, Rab3D is predominantly expressed in peripheral tissues where the other isoforms either are expressed at low levels or are lacking. Thus, the effect of Rab3D deletion should not be influenced by functional compensation, at least not to a major extent. Surprisingly, deletion of Rab3D has no effect on the kinetics or the extent of regulated exocytosis, as documented by our analysis of exocytosis in mast cells and exocrine glands. Thus, we conclude that the function of Rab3D differs from that of Rab3A and from that of the only Rab3 isoform expressed in the nervous system of *C. elegans*. Two alternative explanations are possible. First, Rab3D, despite its sequence similarity to Rab3A, is structurally sufficiently different to interact with different sets of proteins. Such proteins may include the effectors or the proteins responsible for the recruitment of Rab3A and Rab3D to specific subcellular compartments. Differences in localization between Rab3A and Rab3D were suggested by localization studies of RBL and AtT20 cells (9, 49). Second, the interacting proteins may not distinguish between Rab3A and Rab3D, but their expression pattern varies between different tissues, thus determining the specific cellular response to the Rab3 GTP-GDP cycle. For instance, the Rab3A effectors rabphilin and RIM are predominantly expressed in the nervous system, and it is conceivable that peripheral tissues contain other, hitherto-unknown Rab3 effectors. Currently, we cannot distinguish between these possibilities. Interestingly, rabphilin levels were not changed in acinar cells of Rab3D-deficient mice whereas they are reduced in neurons of mice lacking Rab3A (22).

Previous work suggested that Rab3D controls exocytosis in mast cells (49). However, our analysis of mast cell degranulation in Rab3D-deficient mice conclusively shows that neither kinetics, vesicle size, nor the extent of exocytosis is altered. Thus, we conclude that Rab3D has neither a direct nor an indirect effect on mast cell exocytosis. In the study by Roa et al. (49), overexpression of both wild-type and guanine-nucleotide-binding-deficient Rab3D caused a reduction in hexosaminidase release. In light of our data, the specificity of these effects needs to be reconsidered. Although experiments overexpressing proteins are popular, the effects of Rab proteins, either wild type or mutant, need to be interpreted with caution, particularly when they result in a loss of function.

The most conspicuous change in Rab3D-deficient mice is a substantially increased size of the secretory granules, while the intragranular protein concentration appears to be unchanged. It should be noted that the size of the pancreas zymogen granules is variable and depends on physiological and developmental factors. For instance, in starved animals the diameter of zymogen granules is increased by about 20 to 30% (6, 18). We observed a similar increase when comparing starved and fed mice. However, this increase was evident in both wild-type and Rab3D-deficient mice and thus is superimposed on the size difference caused by Rab3D deletion (unpublished observations).

More interestingly, it has been known for many years that during development of the pancreas the size of zymogen granules shrinks around birth (17), i.e., around the time the gland acquires competence for regulated secretion (55). Rab3D is expressed 2 days after the appearance of zymogen granules, but it is not membrane associated until birth (56). In the light of the results described here, it is likely that membrane binding of Rab3D during the time of birth is directly responsible for granular size reduction during development.

How does Rab3D regulate the size of secretory granules? There are two possible explanations for this phenotype. First, the size of condensing vacuoles budding off the trans-Golgi network could be larger. In unstimulated glands, Rab3D is predominantly localized to mature secretory granules with only little labeling of the Golgi or trans-Golgi network region (32). However, upon stimulation for 3 h most of the zymogen granules disappeared and Rab3D was then localized to newly forming secretory vesicles on the trans-Golgi network, which would be compatible with a role in determining the size of condensing vacuoles. According to this scenario, all subsequent maturation steps would be normal, but the initially larger size would carry over to the final maturation steps.

Alternatively, the role of Rab3D may be to downregulate fusion of secretory granules at a step subsequent to the formation of condensing vacuoles. Although not previously reported from exocrine glands, it was suggested earlier not only that secretory granules may have the capacity to undergo homotypic fusion but that such fusion may, at least in some systems, be part of a normal maturation process (54). Such a scenario would be compatible with an inhibitory effect of Rab3 proteins in fusion events as already inferred for Rab3A from the study of Rab3A-deficient mice. The only difference would be that for Rab3D the fusion step controlled by the protein is not exocytosis but rather a preceding step (granule-granule fusion).

In summary, our study investigates the potential role of Rab3D in exocytosis in exocrine glands and mast cells. This study was prompted by the need for an independent in vivo assessment of the function of Rab3D. Many previous studies indicated that Rab3D is central for exocytotic fusion outside of neuronal and endocrine cells, but all of these studies utilized indirect approaches that made it difficult to derive definitive answers. Surprisingly, our data rule out an essential role for Rab3D in exocytosis. Although Rab3D is probably functionally redundant with other Rab3 isoforms, its function is not completely redundant in exocrine cells as shown here because, in the absence of Rab3D, these cells exhibit a clear maturation defect in zymogen granules. Future studies will have to examine the precise genesis of the maturation defect. However, whatever its nature, Rab3D clearly functions differently than previously envisioned.

ACKNOWLEDGMENTS

We thank the staff of the animal care facilities at the Max Planck Institute for Experimental Medicine and the Max Planck Institute for Biophysical Chemistry for invaluable help with blastocyst injection and animal husbandry. We are grateful to H. F. Kern as well as members of R. Jahn's lab for useful comments and critical discussions and patience.

REFERENCES

1. **Alvarez de Toledo, G., R. Fernandez-Chacon, and J. M. Fernandez.** 1993. Release of secretory products during transient vesicle fusion. Nature **363:** 554–558.
2. **An, S. J., N. J. Hansen, A. Hodel, R. Jahn, and J. M. Edwardson.** 2000. Analysis of the association of syncollin with the membrane of the pancreatic zymogen granule. J. Biol. Chem. **275:**11306–11311.
3. **Annaert, W. G., B. Becker, U. Kistner, M. Reth, and R. Jahn.** 1997. Export of cellubrevin from the endoplasmic reticulum is controlled by BAP31. J. Cell Biol. **139:**1397–1410.

4. **Antonin, W., C. Holroyd, D. Fasshauer, S. Pabst, G. F. Von Mollard, and R. Jahn.** 2000. A SNARE complex mediating fusion of late endosomes defines conserved properties of SNARE structure and function. EMBO J. **19:**6453–6464.
5. **Antonin, W., M. Wagner, D. Riedel, N. Brose, and R. Jahn.** 2002. Loss of the zymogen granule protein syncollin affects pancreatic protein synthesis and transport but not secretion. Mol. Cell. Biol. **22:**1545–1554.
6. **Aughsteen, A. A., and G. H. Cope.** 1987. Changes in the size and number of secretion granules in the rat exocrine pancreas induced by feeding or stimulation in vitro. A morphometric study. Cell Tissue Res. **249:**427–436.
7. **Baldini, G., T. Hohl, H. Y. Lin, and H. F. Lodish.** 1992. Cloning of a Rab3 isotype predominantly expressed in adipocytes. Proc. Natl. Acad. Sci. USA **89:**5049–5052.
8. **Baldini, G., P. E. Scherer, and H. F. Lodish.** 1995. Nonneuronal expression of Rab3A: induction during adipogenesis and association with different intracellular membranes than Rab3D. Proc. Natl. Acad. Sci. USA **92:**4284–4288.
9. **Baldini, G., G. Wang, M. Weber, M. Zweyer, R. Bareggi, J. W. Witkin, and A. M. Martelli.** 1998. Expression of Rab3D N135I inhibits regulated secretion of ACTH in AtT-20 cells. J. Cell Biol. **140:**305–313.
10. **Bergmeyer, H. U.** 1974. Methoden der enzymatischen Analyse. Verlag Chemie, Weinheim/Bergstrasse, Germany.
11. **Bernfeld, P.** 1955. Amylase, alpha and beta. Methods Enzymol. **1:**31149–31158.
12. **Bock, J. B., H. T. Matern, A. A. Peden, and R. H. Scheller.** 2001. A genomic perspective on membrane compartment organization. Nature **409:**839–841.
13. **Bordier, C.** 1981. Phase separation of integral membrane proteins in Triton X-114 solution. J. Biol. Chem. **256:**1604–1607.
14. **Chou, J. H., and R. Jahn.** 2000. Binding of Rab3A to synaptic vesicles. J. Biol. Chem. **275:**9433–9440.
15. **Demo, S. D., E. Masuda, A. B. Rossi, B. T. Throndset, A. L. Gerard, E. H. Chan, R. J. Armstrong, B. P. Fox, J. B. Lorens, D. G. Payan, R. H. Scheller, and J. M. Fisher.** 1999. Quantitative measurement of mast cell degranulation using a novel flow cytometric annexin-V binding assay. Cytometry **36:**340–348.
16. **Edelmann, L., P. I. Hanson, E. R. Chapman, and R. Jahn.** 1995. Synaptobrevin binding to synaptophysin: a potential mechanism for controlling the exocytotic fusion machine. EMBO J. **14:**224–231.
17. **Ermak, T. H., and S. S. Rothman.** 1983. Increase in zymogen granule volume accounts for increase in volume density during prenatal development of pancreas. Anat. Rec. **207:**487–501.
18. **Ermak, T. H., and S. S. Rothman.** 1981. Zymogen granules of pancreas decrease in size in response to feeding. Cell Tissue Res. **214:**51–66.
19. **Fasshauer, D., W. Antonin, M. Margittai, S. Pabst, and R. Jahn.** 1999. Mixed and non-cognate SNARE complexes. Characterization of assembly and biophysical properties. J. Biol. Chem. **274:**15440–15446.
20. **Fischer von Mollard, G., B. Stahl, A. Khokhlatchev, T. C. Sudhof, and R. Jahn.** 1994. Rab3C is a synaptic vesicle protein that dissociates from synaptic vesicles after stimulation of exocytosis. J. Biol. Chem. **269:**10971–10974.
21. **Fischer von Mollard, G., B. Stahl, C. Walch-Solimena, K. Takei, L. Daniels, A. Khoklatchev, P. De Camilli, T. C. Sudhof, and R. Jahn.** 1994. Localization of Rab5 to synaptic vesicles identifies endosomal intermediate in synaptic vesicle recycling pathway. Eur. J. Cell Biol. **65:**319–326.
22. **Geppert, M., V. Y. Bolshakov, S. A. Siegelbaum, K. Takei, P. De Camilli, R. E. Hammer, and T. C. Sudhof.** 1994. The role of Rab3A in neurotransmitter release. Nature **369:**493–497.
23. **Geppert, M., Y. Goda, C. F. Stevens, and T. C. Sudhof.** 1997. The small GTP-binding protein Rab3A regulates a late step in synaptic vesicle fusion. Nature **387:**810–814.
24. **Hamill, O. P., A. Marty, E. Neher, B. Sakmann, and F. J. Sigworth.** 1981. Improved patch-clamp techniques for high-resolution current recording from cells and cell-free membrane patches. Pflugers Arch. **391:**85–100.
25. **Hansen, N. J., W. Antonin, and J. M. Edwardson.** 1999. Identification of SNAREs involved in regulated exocytosis in the pancreatic acinar cell. J. Biol. Chem. **274:**22871–22876.
26. **Hooper, M., K. Hardy, A. Handyside, S. Hunter, and M. Monk.** 1987. HPRT-deficient (Lesch-Nyhan) mouse embryos derived from germline colonization by cultured cells. Nature **326:**292–295.
27. **Hummel, B. C.** 1959. A modified spectrophotometric determination of chymotrypsin, trypsin and thrombin. Can. J. Biochem. **37:**1393–1399.
28. **Huttner, W. B., W. Schiebler, P. Greengard, and P. De Camilli.** 1983. Synapsin I (protein I), a nerve terminal-specific phosphoprotein. III. Its association with synaptic vesicles studied in a highly purified synaptic vesicle preparation. J. Cell Biol. **96:**1374–1388.
29. **Iezzi, M., G. Escher, P. Meda, A. Charollais, G. Baldini, F. Darchen, C. B. Wollheim, and R. Regazzi.** 1999. Subcellular distribution and function of Rab3A, B, C, and D isoforms in insulin-secreting cells. Mol. Endocrinol. **13:**202–212.
30. **Iwasaki, K., J. Staunton, O. Saifee, M. Nonet, and J. H. Thomas.** 1997. aex-3 encodes a novel regulator of presynaptic activity in C. elegans. Neuron **18:**613–622.
31. **Iwasaki, K., and R. Toyonaga.** 2000. The Rab3 GDP/GTP exchange factor homolog AEX-3 has a dual function in synaptic transmission. EMBO J. **19:**4806–4816.
32. **Jena, B. P., F. D. Gumkowski, E. M. Konieczko, G. F. von Mollard, R. Jahn, and J. D. Jamieson.** 1994. Redistribution of a rab3-like GTP-binding protein from secretory granules to the Golgi complex in pancreatic acinar cells during regulated exocytosis. J. Cell Biol. **124:**43–53.
33. **Li, C., K. Takei, M. Geppert, L. Daniell, K. Stenius, E. R. Chapman, R. Jahn, P. De Camilli, and T. C. Sudhof.** 1994. Synaptic targeting of rabphilin-3A, a synaptic vesicle Ca^{2+}/phospholipid-binding protein, depends on rab3A/3C. Neuron **13:**885–898. (Erratum, **15:**240, 1995.)
34. **Lindau, M.** 1991. Time-resolved capacitance measurements: monitoring exocytosis in single cells. Q. Rev. Biophys. **24:**75–101.
35. **Martelli, A. M., G. Baldini, G. Tabellini, D. Koticha, and R. Bareggi.** 2000. Rab3A and Rab3D control the total granule number and the fraction of granules docked at the plasma membrane in PC12 cells. Traffic **1:**976–986.
36. **Martelli, A. M., R. Bareggi, G. Baldini, P. E. Scherer, and H. F. Lodish.** 1995. Diffuse vesicular distribution of Rab3D in the polarized neuroendocrine cell line AtT-20. FEBS Lett. **368:**271–275.
37. **Matteoli, M., K. Takei, R. Cameron, P. Hurlbut, P. A. Johnston, T. C. Sudhof, R. Jahn, and P. De Camilli.** 1991. Association of Rab3A with synaptic vesicles at late stages of the secretory pathway. J. Cell Biol. **115:**625–633.
38. **Nadin, C. Y., J. Rogers, S. Tomlinson, and J. M. Edwardson.** 1989. A specific interaction in vitro between pancreatic zymogen granules and plasma membranes: stimulation by G-protein activators but not by Ca^{2+}. J. Cell Biol. **109:**2801–2808.
39. **Nonet, M. L., J. E. Staunton, M. P. Kilgard, T. Fergestad, E. Hartwieg, H. R. Horvitz, E. M. Jorgensen, and B. J. Meyer.** 1997. *Caenorhabditis elegans* rab-3 mutant synapses exhibit impaired function and are partially depleted of vesicles. J. Neurosci. **17:**8061–8073.
40. **Novick, P., and M. Zerial.** 1997. The diversity of Rab proteins in vesicle transport. Curr. Opin. Cell Biol. **9:**496–504.
41. **Oberhauser, A. F., V. Balan, C. L. Fernandez-Badilla, and J. M. Fernandez.** 1994. RT-PCR cloning of Rab3 isoforms expressed in peritoneal mast cells. FEBS Lett. **339:**171–174.
42. **Ohnishi, H., S. A. Ernst, N. Wys, M. McNiven, and J. A. Williams.** 1996. Rab3D localizes to zymogen granules in rat pancreatic acini and other exocrine glands. Am. J. Physiol. **271:**G531–G538.
43. **Ohnishi, H., L. C. Samuelson, D. I. Yule, S. A. Ernst, and J. A. Williams.** 1997. Overexpression of Rab3D enhances regulated amylase secretion from pancreatic acini of transgenic mice. J. Clin. Investig. **100:**3044–3052.
44. **Ostermeier, C., and A. T. Brunger.** 1999. Structural basis of Rab effector specificity: crystal structure of the small G protein Rab3A complexed with the effector domain of rabphilin-3A. Cell **96:**363–374.

44a. **Palade, G.** 1975. Intracellular aspects of the process of protein synthesis. Science **189:**347–358.

45. **Parsons, T. D., J. R. Coorssen, H. Horstmann, and W. Almers.** 1995. Docked granules, the exocytic burst, and the need for ATP hydrolysis in endocrine cells. Neuron **15:**1085–1096.
46. **Pereira-Leal, J. B., and M. C. Seabra.** 2001. Evolution of the Rab family of small GTP-binding proteins. J. Mol. Biol. **313:**889–901.
47. **Raffaniello, R. D., J. Lin, R. Schwimmer, and G. K. Ojakian.** 1999. Expression and localization of Rab3D in rat parotid gland. Biochim. Biophys. Acta **1450:**352–363.
48. **Richards, G. M.** 1974. Modifications of the diphenylamine reaction giving increased sensitivity and simplicity in the estimation of DNA. Anal. Biochem. **57:**369–376.
49. **Roa, M., F. Paumet, J. Le Mao, B. David, and U. Blank.** 1997. Involvement of the ras-like GTPase rab3d in RBL-2H3 mast cell exocytosis following stimulation via high affinity IgE receptors (FcεRI). J. Immunol. **159:**2815–2823.
50. **Scheele, G. A., and G. E. Palade.** 1975. Studies on the guinea pig pancreas. Parallel discharge of exocrine enzyme activities. J. Biol. Chem. **250:**2660–2670.
51. **Schluter, O. M., E. Schnell, M. Verhage, T. Tzonopoulos, R. A. Nicoll, R. Janz, R. C. Malenka, M. Geppert, and T. C. Sudhof.** 1999. Rabphilin knockout mice reveal that rabphilin is not required for rab3 function in regulating neurotransmitter release. J. Neurosci. **19:**5834–5846.
52. **Segev, N.** 2001. Ypt and Rab GTPases: insight into functions through novel interactions. Curr. Opin. Cell Biol. **13:**500–511.
53. **Stroupe, C., and A. T. Brunger.** 2000. Crystal structures of a Rab protein in its inactive and active conformations. J. Mol. Biol. **304:**585–598.
54. **Urbe, S., L. J. Page, and S. A. Tooze.** 1998. Homotypic fusion of immature secretory granules during maturation in a cell-free assay. J. Cell Biol. **143:**1831–1844.
55. **Valentijn, J. A., F. D. Gumkowski, and J. D. Jamieson.** 1996. The expression pattern of rab3D in the developing rat exocrine pancreas coincides with the acquisition of regulated exocytosis. Eur. J. Cell Biol. **71:**129–136.
56. **Valentijn, J. A., D. Sengupta, F. D. Gumkowski, L. H. Tang, E. M. Konieczko, and J. D. Jamieson.** 1996. Rab3D localizes to secretory granules in rat pancreatic acinar cells. Eur. J. Cell Biol. **70:**33–41.
57. **Zerial, M., and H. McBride.** 2001. Rab proteins as membrane organizers. Nat. Rev. Mol. Cell Biol. **2:**107–117.